

Pre-treatment Planning for Hepatic Radiofrequency Ablation

Qiyong Chen and Sinan Müftü
Mechanical and Industrial Eng. Dept.
Northeastern University
Boston, MA 02115-5000, United States
Emails: chen.qiyo@husky.neu.edu and
s.muftu@neu.edu

F.Can Meral and Kemal Tuncali
Department of Radiology
Brigham and Women's Hospital
Harvard Medical School
Boston, MA 02115, United States
Emails: canmeral@gmail.com and
ktuncali@partners.org

Murat Akcakaya
Electrical and Computer Eng. Dept.
University of Pittsburgh
Pittsburgh, PA 15261, United States
Email: akcakaya@pitt.edu

Abstract—We develop a pre-treatment planning method for optimum hepatic radiofrequency (RF) ablation. In conventional methods, pre-treatment planning is minimal and for a specific tumor size, it only includes reading pre-specified treatment length and input voltage values from a look-up table that lists experimentally obtained ablation parameters. Such planning, in order to assure certain level of cell death, usually results in more healthy cell damage than desired. Different than the conventional methods, here, we develop a model-based pre-treatment optimal planning framework. As an example, we use 1-D axisymmetric tissue geometry and over this geometry, we solve Pennes' bioheat and Laplace equations to model the RF heating. Using the solutions of these equations, we define constrained nonlinear optimization problems to achieve specific temperature profiles in certain areas of the tissue. Results demonstrate that compared to the conventional methods, our approach significantly improves the healthy tissue preservation.

I. INTRODUCTION

For hepatic tumors, Radiofrequency (RF) ablation has been a widely employed treatment alternative to surgical resection [1], [2], [3], [4], [5], [6], [7]. When applied to a tissue, alternating electrical current in the RF range (450–500 kHz) causes temperature increase without neuromuscular excitation [8], [9], [7]. Depending on the size of the tumor, current ablation strategy includes the application of a constant voltage level over a predetermined treatment duration (typically between 5 – 30 minutes) [10], [11].

To achieve a desired level of cell death, constant voltage strategy may result in an irreversible healthy tissue damage. To circumvent this, different studies focused on (1) finding an appropriate electrode voltage range [12], [13], [14], (2) positioning of ablation probes [15], [16], [17], [18], and (3) the effects of treatment duration on tissue damage [19], [20], [12]. However, there is no systematic way to control the amount of energy received by different volumes of tissue; and, research into *control* of RF ablation procedure is still very limited. For example, Haemmerich et al. modeled a PI controller to keep the electrode tip temperature at a target level (100° C) [21], but controlling

the temperature of other positions was not considered. In our work, while manipulating the entire temperature history and tissue damage level of certain positions in the target tissue, we present a *pre-operative treatment planning* based on multiple point constraint optimization.

II. RF HEATING MODEL

A. Bioheat Equation

Heat transfer in tissue is governed by the bioheat equation [12],

$$\rho c \frac{\partial T}{\partial t} = \nabla \cdot (\kappa \nabla T) + q - Q_p \quad (1)$$

where T is tissue temperature, ρ is mass density, c is heat capacity, κ is thermal conductivity of the tissue. Internal heat generation due to resistive heating and heat loss due to blood perfusion are represented as a distributed source q and sink Q_p , respectively. Tissue heating in RF ablation is a resistive heating process, modeled by the Joule heating relationship [22], [23], [24], [12],

$$q = \sigma(\nabla V)^2 \quad (2)$$

where σ is electrical conductivity of the tissue, ∇ is gradient operator. As frequency of the electrical potential V is much faster than the characteristic time scale of heat transfer, it can be obtained at steady state, by using,

$$\nabla \cdot (\sigma \nabla V) = 0. \quad (3)$$

Heat loss Q_p due to blood perfusion is of the following form [20],

$$Q_p = h_b(T - T_b) \quad (4)$$

where h_b is the convective heat transfer coefficient, T_b is blood temperature. The convective heat transfer coefficient can be calculated as $h_b = \omega_b \rho_b c_b$, where ρ_b and c_b are the mass density and specific heat of blood, respectively, and ω_b is perfusion coefficient [25].

B. 1D Axisymmetric Model

In this manuscript, to demonstrate the pre-treatment optimization framework, we consider the 1D axisymmetric geometry illustrated in Figure 1. In this geometry, the temperature is a function of time and radial position ($T = T(r, t)$). Inner and outer boundaries of the solution domain are located at r_i and r_o where r_i represents the location of the electrode tip (ET) (r_{KZ} , r_{PZ} , and r_H are defined later in Section III).

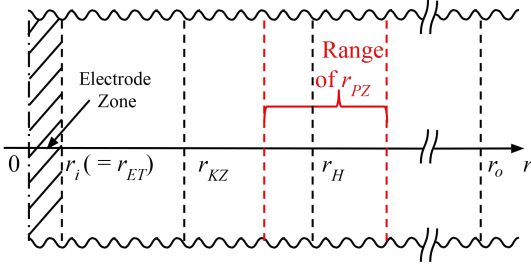


Fig. 1: Axisymmetric cylindrical geometry

The electric potential at the electrode tip is specified as $V(r_i) = V_i$, and, electric potential at outer boundary is zero, i.e. $V(r_o, t) = 0$. Then, electrical potential variation can be found as follows,

$$V(r) = \frac{V_i}{\ln(\frac{r_i}{r_o})} \ln(\frac{r}{r_o}). \quad (5)$$

Considering the electrical potential calculated above, the bioheat equation in polar coordinates becomes,

$$\frac{1}{\alpha} \frac{\partial T}{\partial t} = \frac{1}{r} \frac{\partial}{\partial r} \left(r \frac{\partial T}{\partial r} \right) - \frac{h_b}{\kappa} (T - T_b) + \frac{g}{\kappa} \frac{1}{r^2} \quad (6)$$

where g ($= \sigma(V_i / \ln(r_i/r_o))^2$) represents energy input into the system and α ($= \kappa/\rho c$) is the thermal diffusivity. Inner boundary of the solution domain is in temperature equilibrium [13] as the thermal mass of the probe is negligible compared to the surrounding tissue, while the heat flux is negligible at the outer boundary [26]. These conditions are expressed mathematically as follows,

$$\frac{\partial T}{\partial r} \Big|_{r=r_i} = \frac{\partial T}{\partial r} \Big|_{r=r_o} = 0. \quad (7)$$

In addition, the initial temperature distribution at time $t = 0$ is specified as follows,

$$T(r, 0) = T^{(0)}(r) = T^{(in)}(r). \quad (8)$$

The material properties are assumed to be constant in order to get a closed form solution to the bioheat equation (6) subjected to conditions (7) - (8).

Since equation (6) is a non-homogeneous linear partial differential equation with homogeneous boundary and initial conditions, we use the eigenfunction expansion method

to obtain a solution [27]. Accordingly, we set the anticipated form of the solution to (6) as a series summation of separable functions as follows,

$$T(r, t) = \sum_{n=1}^{\infty} a_n(t) \cdot \phi_n(r) \quad (9)$$

where $\phi_n(r)$ are eigenfunctions with the corresponding eigenvalues λ_n . In order to find the eigenvalues and eigenfunctions, we first solve the homogeneous problem corresponding to (6). In this solution, we use the unknown variable as U instead of T to differentiate the homogeneous problem from the original non-homogeneous one as follows

$$\frac{1}{\alpha} \frac{\partial U}{\partial t} = \frac{1}{r} \frac{\partial}{\partial r} \left(r \frac{\partial U}{\partial r} \right) - \frac{h_b}{\kappa} U \quad (10)$$

We observe that (10) is a partial differential equation separable in time and space; therefore, we employ $U(r, t) = G(t) \cdot \phi(r)$ in (10) and obtain,

$$\frac{1}{\alpha} \phi(r) \frac{\partial G(t)}{\partial t} = \left(\frac{\partial^2 \phi(r)}{\partial r^2} + \frac{1}{r} \frac{\partial \phi}{\partial r} \right) G(t) - \frac{h_b}{\kappa} G(t) \phi(r) \quad (11)$$

$$\Rightarrow \frac{1}{\alpha} \frac{1}{G} \frac{\partial G}{\partial t} = \frac{1}{\phi} \left(\frac{\partial^2 \phi}{\partial r^2} + \frac{1}{r} \frac{\partial \phi}{\partial r} - \frac{h_b}{\kappa} \phi \right) = -\lambda. \quad (12)$$

First, rewriting (12) as a regular Sturm-Liouville eigenvalue problem, we obtain [27],

$$\frac{\partial^2 \phi}{\partial r^2} + \frac{1}{r} \frac{\partial \phi}{\partial r} + \left(\lambda - \frac{h_b}{\kappa} \right) \phi = 0. \quad (13)$$

Next, multiplying (13) with r^2 , we have

$$r^2 \frac{\partial^2 \phi}{\partial r^2} + r \frac{\partial \phi}{\partial r} + \left[\left(\lambda - \frac{h_b}{\kappa} \right) r^2 - 0 \right] \phi = 0. \quad (14)$$

Then, assigning $z = \sqrt{\lambda - \frac{h_b}{\kappa}} r$, (14) becomes

$$z^2 \frac{\partial^2 \phi}{\partial z^2} + z \frac{\partial \phi}{\partial z} + (z^2 - 0) \phi = 0 \quad (15)$$

We observe that (15) is a zeroth-order Bessel's equation [27]. Therefore, we consider the general solution form for (15) as $\phi(r) = c_1 J_0(\lambda' r) + c_2 Y_0(\lambda' r)$, with $\lambda' = \sqrt{\lambda - \frac{h_b}{\kappa}}$. Then, following (7), we rewrite the corresponding boundary conditions as, $\phi'(r_i) = 0$ and $\phi'(r_o) = 0$ which accordingly lead to

$$\begin{aligned} c_1 \lambda' J_1(\lambda' r_i) + c_2 \lambda' Y_1(\lambda' r_i) &= 0 \\ c_1 \lambda' J_1(\lambda' r_o) + c_2 \lambda' Y_1(\lambda' r_o) &= 0 \end{aligned} \quad (16)$$

In order to obtain the eigenvalues, we calculate the Wronskian of the system defined in (16),

$$W = (\lambda')^2 \cdot J_1(\lambda' r_i) \cdot Y_1(\lambda' r_o) - (\lambda')^2 \cdot J_1(\lambda' r_o) \cdot Y_1(\lambda' r_i). \quad (17)$$

Regarded as a function of λ , (17) has an infinite number of roots, λ_n for $n = 1, \dots, \infty$, which are the eigenvalues of

the system. Accordingly, the corresponding eigenfunctions are

$$\phi_n(r) = J_0(\lambda'_n r) - \frac{J_1(\lambda'_n r_0)}{Y_1(\lambda'_n r_0)} Y_0(\lambda'_n r) \quad (18)$$

for all $n > 1$ values. Note that $\phi_1(r) = 1$ is a special case of the eigenfunctions.

Recall that we assume in (9) that $T(r, t) = \sum_{n=1}^{\infty} a_n(t) \cdot \phi_n(r)$. From (17) and (18), we obtain $\phi_n(r)$. In the next step, we demonstrate how to compute $a_n(t)$. Using (9) in (12), we obtain the following relationships

$$\begin{cases} \frac{\partial T}{\partial t} = \sum_{n=1}^{\infty} \frac{da_n(t)}{dt} \phi_n(r) \\ \frac{\partial^2 T}{\partial r^2} + \frac{1}{r} \frac{\partial T}{\partial r} - \frac{h_b}{\kappa} T = - \sum_{n=1}^{\infty} a_n(t) \phi_n(r) \lambda_n \end{cases} \quad (19)$$

Using (19) in (6), we write

$$\sum_{n=1}^{\infty} \left[\frac{1}{\alpha} \frac{da_n(t)}{dt} + \lambda_n a_n(t) \right] \phi_n(r) = \frac{g}{\kappa} \frac{1}{r^2} + \frac{h_b}{\kappa} T_b. \quad (20)$$

Noting that ϕ_n is orthogonal to ϕ_m , we compute [27],

$$\frac{1}{\alpha} \frac{da_n(t)}{dt} + \lambda_n a_n(t) = \frac{\int_{r_i}^{r_o} \left(\frac{g}{\kappa} \frac{1}{r^2} + \frac{h_b}{\kappa} T_b \right) \phi_n(r) r dr}{\int_{r_0}^{r_i} \phi_n^2(r) r dr} \equiv q_n \quad (21)$$

where q_n is the generalized Fourier coefficients of the term $\left(\frac{g}{\kappa} \frac{1}{r^2} + \frac{h_b}{\kappa} T_b \right)$ with respect to $\phi_n(r)$ [27].

Next, we solve (21), which is a linear non-homogeneous first order ordinary differential equation, to obtain $a_n(t)$

$$e^{\lambda_n \alpha t} \left[\frac{da_n(t)}{dt} + \lambda_n \alpha a_n(t) \right] = \frac{d}{dt} (a_n(t) e^{\lambda_n \alpha t}) = q_n \alpha e^{\lambda_n \alpha t} \quad (22)$$

where $e^{\lambda_n \alpha t}$ is the integrating factor. Then integrating (22) from 0 to t , we find

$$a_n(t) e^{\lambda_n \alpha t} - a_n(0) = \int_0^t q_n \alpha e^{\lambda_n \alpha \tau} d\tau \quad (23)$$

$$\Rightarrow a_n(t) = \left[a_n(0) - \frac{q_n}{\lambda_n} \right] e^{-\lambda_n \alpha t} + \frac{q_n}{\lambda_n}. \quad (24)$$

In order to compute $a_n(0)$, we apply the initial condition $T(r, 0) = T^{(in)}(r)$ to (9),

$$\sum_{n=1}^{\infty} a_n(0) \phi_n(r) = T^{(0)}(r). \quad (25)$$

Again recalling that ϕ_n and ϕ_m are orthogonal to each other, $a_n(0)$ is computed as [27]

$$a_n(0) = \frac{\int_{r_i}^{r_o} T^{(in)}(r) \phi_n(r) r dr}{\int_{r_i}^{r_o} \phi_n^2(r) r dr}. \quad (26)$$

Finally, using (17), (18), (24) and (26), we calculate λ_n , $a_n(t)$ and $\phi_n(r)$ and obtain the solution to the 1-D axisymmetric problem as

$$T(r, t) = \sum_{n=1}^{\infty} \left\{ \epsilon_n^0 e^{-\lambda_n \alpha t} + \xi_n^0 (1 - e^{-\lambda_n \alpha t}) \right\} \phi_n(r) \quad (27)$$

where $\epsilon_n^0 = \frac{\int_{r_i}^{r_o} T^{(0)}(r) \phi_n(r) r dr}{\int_{r_i}^{r_o} \phi_n^2(r) r dr}$, $\xi_n^0 = \frac{\int_{r_i}^{r_o} \left(\frac{g}{\kappa} \frac{1}{r^2} + \frac{h_b}{\kappa} T_b \right) \phi_n(r) r dr}{\lambda_n \int_{r_i}^{r_o} \phi_n^2(r) r dr}$ such that $g (= \sigma(V_i / \ln(r_i/r_o))^2)$ and accordingly V_i are constant throughout the ablation. In the rest of this section, we demonstrate how to modify the solution in (27) to obtain temperature variation when V_i is varied.

We next evaluate the continuous temperature variation $T(r, t)$ at discrete temporal and radial positions $T_j^{(k)}$, where j refers to a radial position on a discretized spatial grid, and (k) refers to the k^{th} time step. In this work, the solution domain $[r_i, r_o]$ is divided into N equally spaced intervals of length $\Delta r = (r_o - r_i)/N$. Transformation $r = r_i + (j - 1)\Delta r$ for $j = [1, N + 1]$ is used to map the continuous and discrete domains. Similarly the duration of treatment τ is divided into M equally spaced time intervals, with the transformation $t = (k - 1)\Delta t$ for $k = [1, M + 1]$, where $\Delta t = \tau/M$.

First, while solving for the consecutive time intervals, from time step $(k - 1)$ to (k) , equation (27) can be generalized for a general initial condition $T^{(k-1)}(r)$ from time step $(k - 1)$ as follows,

$$T^{(k)}(r) = \sum_{n=1}^{\infty} \left\{ \epsilon^{(k-1)}(r) e^{-\lambda_n \alpha \Delta t} + \xi_n^{(k)} (1 - e^{-\lambda_n \alpha \Delta t}) \right\} \phi_n(r) \quad (28)$$

where $\epsilon^{(k-1)}(r) = \frac{\int_{r_i}^{r_o} T^{(k-1)}(r) \phi_n(r) r dr}{\int_{r_i}^{r_o} \phi_n^2(r) r dr}$ and $\xi_n^{(k)} = \frac{\int_{r_i}^{r_o} \left(\frac{g^{(k)}}{\kappa} \frac{1}{r^2} + \frac{h_b}{\kappa} T_b \right) \phi_n(r) r dr}{\lambda_n \int_{r_i}^{r_o} \phi_n^2(r) r dr}$ such that $T^{(k)}(r)$ is the

radial temperature profile at the end of the k^{th} time interval, and $g^{(k)} = \sigma(V_i^{(k)} / \ln(r_i/r_o))^2$ with $V_i^{(k)}$ as the input electrical potential between time steps $k - 1$ and k . We assume $V_i^{(k)}$ is constant within each interval but can change from one interval to another.

Note that when discretized in space, calculation of temperature on the spatially discretized grid affects only the first term on the right hand side of the equation (28)

$(\epsilon^{(k-1)}(r))$ as follows,

$$T_j^{(k)} = \xi_n^{(k)} \left(1 - e^{-\lambda_n \alpha \Delta t} \right) \phi_n(r_j) + \sum_{n=1}^{\infty} e^{-\lambda_n \alpha \Delta t} \phi_n(r_j) \left[\frac{\Delta r}{2} \sum_{l=1}^N (T_l^{(k-1)} + T_{l+1}^{(k-1)}) \phi_n(r_l) (r_l) \right] \int_{r_i}^{r_o} \phi_n^2(r) r dr \quad (29)$$

where $r_l = r_i + (l - \frac{1}{2}) \Delta r$, and trapezoidal rule is used to approximate the integral involving $T^{(k-1)}(r) = T_j^{(k-1)}$ [28].

III. OPTIMAL PLANNING

In conventional RF treatments, a constant input voltage is used for a predetermined duration to ablate a designated “kill-zone”. While the goal in this work is not only to guarantee a completely ablated “kill-zone”, but also to preserve as much healthy tissue as possible.

The treatment domain is divided into three different zones with key demarcation boundaries, as depicted in Figure 1. We employ the Arrhenius index to define the treatment domain partitions [18], [26], [20], [12], [29], [25], [19].

$$\Omega(T) = \ln \frac{c(0)}{c(t)} = F \int_0^t \exp\left(\frac{-\Delta E}{RT(t^*)}\right) dt^* \quad (30)$$

where $c(0)$ is the original concentration of living cells [30], R ($= 8.314 \text{ J/mol}\cdot\text{K}$) is the universal gas constant [19], F is the “frequency” coefficient and ΔE is the energy of initiation of irreversible ablation reaction. Arrhenius index represents the effect of temperature history at a given position and thus has been shown to be more effective than using temperature to monitor tissue damage [31], [32], [33], [34], [16], [12], [29]. For liver tissue under RF current $F = 7.39 \times 10^{39} \text{ s}^{-1}$ and $\Delta E = 2.577 \times 10^5 \text{ J/mol}$ [35]. Damage integral value $\Omega = 1$ remarks a 63% probability of cell death, whereas $\Omega = 4.6$ refers to a 99% probability of cell death. The significance of $\Omega = 1$ has been reported as the point at which tissue coagulation first occurs and blood perfusion ceases [12], [20], [19]. In this work, $\Omega = 1$ and $\Omega = 4.6$ are used to determine the boundaries of healthy and dead (kill zone) tissue, respectively.

Accordingly, in Figure 1 the *kill zone* spans the range $r_{ET} \leq r \leq r_{KZ}$. The kill-zone radius r_{KZ} is greater than the tumor radius, including a safety margin. The *heat affected zone* is located in the range $r_{KZ} \leq r \leq r_H$, where r_H indicates the *healthy zone boundary* ($\Omega = 1$). The *healthy zone* lies in the range $r_H \leq r \leq r_o$ where $\Omega < 1$. In addition, we define a *preservation zone boundary* r_{PZ} where an optimization constraint is assigned. This boundary is set to be several millimeters larger than r_{KZ} . Note that r_{PZ} is used as a variable to improve the treatment outcome as described below.

Following the partitioning in Figure 1, we desire to achieve a specific temperature value in a specific location of the target geometry while also minimizing the input voltage to avoid excessive tissue heating. We consider a

cost function inspired by linear quadratic regulator theory [36] as follows,

$$J(\mathbf{V}) = \sum_{k=1}^{M+1} \|T_{KZ}^{(k)}\|^2. \quad (31)$$

where $\mathbf{V} = [V_i^{(1)}, \dots, V_i^{(M)}]^T$ with $V_i^{(k)}$ as the input voltage at the k^{th} time step, and T_{KZ}^k is the temperature at the kill-zone boundary (at r_{KZ}) and it is computed using (29).

To avoid tissue charring and minimize thermal injury in healthy tissue while guaranteeing total ablation of the kill zone, we define the following three linear constraints at r_{ET} , r_{PZ} and r_{KZ} , respectively.

$$\begin{aligned} C1 : T(r_{ET}, t) &\leq T_{ET}^*, \text{ for } t \leq \tau \\ C2 : T(r_{PZ}, t) &\leq T_{PZ}^*, \text{ for } t \leq \tau \\ C3 : T(r_{KZ}, t) &\geq T^*(r_{KZ}, t), \text{ for } t \leq \tau \end{aligned} \quad (32)$$

where the constraints T_{ET}^* and T_{PZ}^* are temperature upper bounds at r_{ET} and r_{PZ} , respectively. T_{ET}^* value is selected to prevent tissue charring; T_{PZ}^* is chosen to preserve healthy tissue. In the third constraint, the tissue temperature at the kill zone boundary $T(r_{KZ}, t)$ is constrained to be above a time-dependent temperature profile $T^*(r_{KZ}, t)$ for the entire treatment duration. These temperature constraints are chosen such that at the end of τ , $\Omega(r_{KZ})$ is greater than 4.6.

Note that from (28) and (29), we observe that (31) is a quadratic function of \mathbf{V} . Therefore, together with the linear constraints defined in (32), the optimal planning is formulated as a convex quadratic constrained optimization problem. A feasible solution to this problem will be globally optimal [37]. We use MATLAB’s optimization toolbox to solve this convex problem.

IV. RESULTS AND DISCUSSION

Using the 1D axisymmetric geometry, we compare the healthy tissue preservation properties of the proposed pre-treatment and conventional plans. In our simulations, we use the geometry partitioning and optimization parameters and material properties as listed in Table I. For simplification, we assume that the material properties are uniform and constant in our simulations. Temperature dependent material properties is the subject of our future work.

To evaluate the performance we evaluate the volume ($V_H = \pi(r_o^2 - r_H^2)$) of remaining healthy tissue at the end of treatment, where r_H is the tissue radius where $\Omega = 1$ at the end of treatment. Volume of retained healthy tissue with optimization is compared to that obtained with the conventional treatment by using the normalized variable,

$$\Delta \bar{V} = \frac{(r_H^c)^2 - (r_H^{opt})^2}{r_{KZ}^2} \times 100 \quad (33)$$

where r_H^c is the radius of the healthy region obtained by using the conventional treatment protocol. The conventional treatment constitutes of a constant voltage applied for a fixed duration. In this case for the parameters given in Table I we find that 20.68 Volts is required to reach $\Omega = 4.6$ at the kill zone boundary ($r_{KZ} = 5$ mm) in 1000 seconds. The resulting healthy zone is found to lie in $r \geq r_H$ (= 9.4 mm) where $\Omega \leq 1$, at $t \geq \tau$.

Using a step-wise increasing temperature constraint $T^*(r_{KZ}, t)$ as shown in Figure 2b in C3 of (32), we calculate the optimal voltage sequence (treatment plan), as also shown in Figure 2b. We observe that the optimal voltage sequence calculated by the optimizer closely follows the step variation with the exception that voltage spikes occur between the steps. Resulting temperature variation (Figure 2a) also reflects the temperature spikes, but only near the electrode.

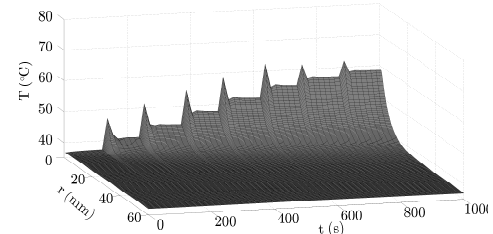
Note that the second constraint (C2) can be modified to influence the treatment outcome for fixed C1 and C3. In particular, different C2 values change the volume of the preserved tissue. Table II shows the normalized change in healthy tissue volume $\Delta\bar{V}$. Recall that r_{PZ} and T_{PZ} are the preservation zone boundary and temperature upperbound at that boundary respectively. Not that the r_{PZ} , T_{PZ}^* combinations for which an optimized solution was not feasible are left unmarked. For the parameters that give rise to feasible solutions, we observe around %50 increase in healthy tissue preservation. Due to computational simplifications the spatial discretization is chosen to be sparse and the T_{PZ} and r_{PZ} are chosen in small ranges. These choices gave rise to identical normalized improvement.

TABLE I: Parameters and material properties adopted in the simulated conventional treatments and optimization cases. Material properties are assumed to be uniform and constant in this work

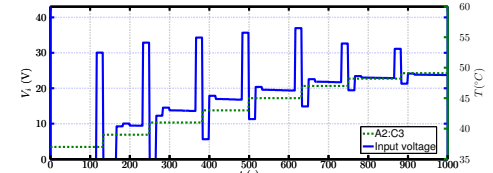
r_o	Domain size (mm)	60
r_{ET}	Electrode tip radius (mm)	1
r_{KZ}	Kill-zone radius (mm)	5
r_{PZ}	Preservation-zone radius (mm)	7 - 13
τ	Duration of treatment (s)	1000
T_b	Body temperature ($^{\circ}$ C)	37
T_{PZ}^*	Preservation-zone boundary temperature limit ($^{\circ}$ C)	40 - 43
T_{ET}^*	Electrode tip temperature limit ($^{\circ}$ C)	80
N	Number of spatial intervals	200
M	Number of temporal intervals	60
κ	Thermal conductivity (w/K·m)	0.502
σ	Electric conductivity (S/m)	0.148
ρ	Mass density (kg/m^3)	1060
ρ_b	Mass density of blood (kg/m^3)	1000
c	Specific heat of tissue ($\text{J}/\text{kg}\cdot\text{C}$)	3600
c_b	Specific heat of blood (kg/m^3)	4180
ω_b	Blood perfusion coefficient (s^{-1})	6.4×10^{-3}
ϵ	Blood perfusion weighing factor [25]	0.6

V. SUMMARY AND CONCLUSION

This work presents the first attempt to optimize input voltage variation as a pre-operative planning sequence for hepatic radiofrequency ablation. Unlike previous studies which used constant voltage or simple electrode-tip temperature controlled model, this work demonstrated the possibility of controlling certain position's historical



(a) Temperature surface of A1



(b) Input sequence of A1

Fig. 2: Resulting temperature surface and input voltage variation plots of a sample case. (a) Temperature variation as a function of time and location and (b) optimized voltage sequence. The following parameters were used $r_{KZ} = 5$ mm, $r_{PZ} = 12$ mm, $T_{PZ}^* = 41.6$ $^{\circ}$ C along with those listed in Table I

temperature profile and resulting local tissue damage level. Pre-operational input sequence optimization was implemented to achieve desirable RF ablation strategy which could guarantee a complete ablation of the designated “kill zone” while retaining a considerable amount of healthy tissue thermal-injury free. The methods outlined here can be expanded to 3D realistic scenarios with relative ease. It is expected that by incorporating an optimization method the RF ablation treatments can become more effective. The methodology used in this work would be applicable to cryo treatments of tumors with relative minor changes. The current work assumes that material properties are constant and uniform throughout the solution domain. Future work will relax this assumption. Moreover, future work will focus on phantom studies to validate the method on more complex geometries.

REFERENCES

- [1] J. P. McGahan, P. D. Browning, J. M. Brock, and H. Tesluk, “Hepatic ablation using radiofrequency electrocautery,” *Investigative Radiology*, vol. 25, no. 3, pp. 267–270, 1990.
- [2] L. Solbiati, S. N. Goldberg, T. Ierace, T. Livraghi, F. Meloni, M. Dellanoce, S. Sironi, and G. S. Gazelle, “Hepatic metastases: percutaneous radio-frequency ablation with cooled-tip electrodes.” *Radiology*, vol. 205, no. 2, pp. 367–373, Nov. 1997.
- [3] S. Rossi, E. Buscarini, F. Garbagnati, M. Di Stasi, P. Quarrelli, M. Rago, A. Zangrandi, S. Andreola, D. Silverman, and L. Buscarini, “Percutaneous treatment of small hepatic tumors by an expandable RF needle electrode.” *American Journal of Roentgenology*, vol. 170, no. 4, pp. 1015–1022, Apr. 1998.
- [4] S. A. Curley, F. Izzo, P. Delrio, L. M. Ellis, J. Granchi, P. Valpone, F. Fiore, S. Pignata, B. Daniele, and F. Cremona, “Radiofrequency ablation of unresectable primary and metastatic hepatic malignancies,” vol. 230, pp. 1–8, Jul. 1999.
- [5] S. N. Goldberg, G. S. Gazelle, and P. R. Mueller, “Thermal ablation therapy for focal malignancy: A unified approach to underlying principles, techniques, and diagnostic imaging guidance,” *American journal of roentgenology*, vol. 174, no. 2, pp. 323 – 331, 2000.

TABLE II: Improvement in preserved tissue volume as measured by ΔV

		T_{PZ}^* (°C)															
		40.0	40.2	40.4	40.6	40.8	41.0	41.2	41.4	41.6	41.8	42.0	42.2	42.4	42.6	42.8	43
r_{PZ} (mm)	7																49.01
	8																49.01
	9																49.01
	10																49.01
	11																49.01
	12																49.01
	13	49.01	49.01	49.01	49.01	49.01	49.01	49.01	49.01	49.01	49.01	49.01	49.01	49.01	49.01	49.01	49.01

- [6] B. Bowles, J. Machi, W. L. Limm, R. Severino, A. J. Oishi, N. L. Furumoto, L. L. Wong, and R. H. Oishi, "Safety and efficacy of radiofrequency thermal ablation in advanced liver tumors," *Arch. Surg.*, vol. 136, no. 8, pp. 864–869, Aug. 2001.
- [7] J. P. McGahan and G. D. Dodd III, "Radiofrequency ablation of the liver: Current status," *American Journal of Roentgenology*, vol. 176, no. 1, pp. 3 – 16, 2001.
- [8] M. d'Arsonval, "Action physiologique des courants alternatifs," *CR Soc Biol*, vol. 43, pp. 283–286, 1891.
- [9] Y. Ni, S. Mulier, Y. Miao, L. Michel, and G. Marchal, "A review of the general aspects of radiofrequency ablation," *Abdominal imaging*, vol. 30, no. 4, pp. 381–400, 2005.
- [10] H. Rhim, S. N. Goldberg, G. D. Dodd, L. Solbiati, H. K. Lim, M. Tonolini, and O. K. Cho, "Essential techniques for successful radio-frequency thermal ablation of malignant hepatic tumors 1," *Radiographics*, vol. 21, no. suppl_1, pp. S17–S35, 2001.
- [11] E. J. Patterson, C. H. Scudamore, D. A. Owen, A. G. Nagy, and A. K. Buczkowski, "Radiofrequency ablation of porcine liver in vivo: effects of blood flow and treatment time on lesion size," *Annals of surgery*, vol. 227, no. 4, p. 559, 1998.
- [12] I. A. Chang and U. D. Nguyen, "Thermal modeling of lesion growth with radiofrequency ablation devices," *Biomedical engineering online*, vol. 3, no. 1, p. 27, 2004.
- [13] I. Chang, "Finite element analysis of hepatic radiofrequency ablation probes using temperature-dependent electrical conductivity," *Biomedical engineering online*, vol. 2, no. 1, p. 12, 2003.
- [14] D. E. Haines, "Determinants of lesion size during radiofrequency catheter ablation: The role of electrode-tissue contact pressure and duration of energy delivery," *Journal of Cardiovascular Electrophysiology*, vol. 2, no. 6, pp. 509–515, 1991.
- [15] D. Haemmerich, A. Wright, D. Mahvi, F. Lee Jr, and J. Webster, "Hepatic bipolar radiofrequency ablation creates coagulation zones close to blood vessels: a finite element study," *Medical and Biological Engineering and Computing*, vol. 41, no. 3, pp. 317–323, 2003.
- [16] D. Haemmerich, S. Tungjikusolmun, T. Staelin, F. T. Lee Jr, D. M. Mahvi, and J. G. Webster, "Finite-element analysis of hepatic multiple probe radio-frequency ablation," *Biomedical Engineering, IEEE Transactions on*, vol. 49, no. 8, pp. 836–842, 2002.
- [17] C. Villard, L. Soler, and A. Gangi, "Radiofrequency ablation of hepatic tumors: simulation, planning, and contribution of virtual reality and haptics," *Computer Methods in Biomechanics and Biomedical Engineering*, vol. 8, no. 4, pp. 215–227, 2005.
- [18] C.-C. Chen, M. I. Miga, and R. L. Galloway, "Optimizing electrode placement using finite-element models in radiofrequency ablation treatment planning," *Biomedical Engineering, IEEE Transactions on*, vol. 56, no. 2, pp. 237–245, 2009.
- [19] R. Barauskas, A. Gulbinas, and G. Barauskas, "Investigation of radiofrequency ablation process in liver tissue by finite element modeling and experiment," *Medicina (Kaunas)*, vol. 43, no. 4, pp. 310–325, 2007.
- [20] R. Barauskas, A. Gulbinas, T. Vanagas, and G. Barauskas, "Finite element modeling of cooled-tip probe radiofrequency ablation processes in liver tissue," *Computers in biology and medicine*, vol. 38, no. 6, pp. 694–708, 2008.
- [21] D. Haemmerich and J. G. Webster, "Automatic control of finite element models for temperature-controlled radiofrequency ablation," *Biomedical engineering online*, vol. 4, no. 1, p. 42, 2005.
- [22] J. A. López-Molina, M. J. Rivera, M. Trujillo, F. Burdío, J. L. Lequerica, F. Hornero, and E. J. Berjano, "Assessment of hyperbolic heat transfer equation in theoretical modeling for radiofrequency heating techniques," *The open Biomedical engineering journal*, vol. 2, p. 22, 2008.
- [23] M. Trujillo, M. Rivera, J. López Molina, and E. Berjano, "Effect of the thermal wave in radiofrequency ablation modeling: An analytical study," *Math. Med. Biol.*, vol. 26, no. 3, pp. 187–200, 2009.
- [24] D. Panescu, J. Whayne, S. Fleischman, M. Mirotznik, D. Swanson, and J. Webster, "Three-dimensional finite element analysis of current density and temperature distributions during radiofrequency ablation," *IEEE Transactions on Biomedical Engineering*, vol. 42, no. 9, pp. 879 –890, Sep. 1995.
- [25] M. E. Ulucakli and C. S. Lavery, "The effect of perfusion rate on the radiofrequency ablation of liver tumors," in *ASME 2013 International Mechanical Engineering Congress and Exposition*. American Society of Mechanical Engineers, 2013, pp. V03BT03A040–V03BT03A040.
- [26] T. Kröger, I. Altrogge, T. Preusser, P. L. Pereira, D. Schmidt, A. Weihusen, and H.-O. Peitgen, "Numerical simulation of radio frequency ablation with state dependent material parameters in three space dimensions," in *Medical Image Computing and Computer-Assisted Intervention–MICCAI 2006*. Springer, 2006, pp. 380–388.
- [27] R. Haberman, *Elementary Applied Partial Differential Equations With: Fourier Series and Boundary Value Problems*, third edition ed. Prentice Hall, 1998.
- [28] K. E. Atkinson, *An introduction to numerical analysis*. John Wiley & Sons, 2008.
- [29] E. J. Berjano, "Theoretical modeling for radiofrequency ablation: state-of-the-art and challenges for the future," *Biomedical engineering online*, vol. 5, no. 1, p. 24, 2006.
- [30] I. A. Chang, "Considerations for thermal injury analysis for rf ablation devices," *The open biomedical engineering journal*, vol. 4, p. 3, 2010.
- [31] D. Haemmerich, A. Wright, D. Mahvi, F. Lee Jr, and J. Webster, "Hepatic bipolar radiofrequency ablation creates coagulation zones close to blood vessels: a finite element study," *Medical and Biological Engineering and Computing*, vol. 41, no. 3, pp. 317–323, 2003.
- [32] D. Haemmerich, L. Chachati, A. S. Wright, D. M. Mahvi, F. T. Lee Jr, and J. G. Webster, "Hepatic radiofrequency ablation with internally cooled probes: effect of coolant temperature on lesion size," *Biomedical Engineering, IEEE Transactions on*, vol. 50, no. 4, pp. 493–500, 2003.
- [33] Z. Wang, I. Aarya, M. Gueorguieva, D. Liu, H. Luo, L. Manfredi, L. Wang, D. McLean, S. Coleman, S. Brown *et al.*, "Image-based 3d modeling and validation of radiofrequency interstitial tumor ablation using a tissue-mimicking breast phantom," *International journal of computer assisted radiology and surgery*, vol. 7, no. 6, pp. 941–948, 2012.
- [34] S. Tungjikusolmun, T. Staelin, D. Haemmerich, J.-Z. Tsai, H. Cao, J. G. Webster, F. T. Lee Jr, D. M. Mahvi, and V. R. Vorperian, "Three-dimensional finite-element analyses for radiofrequency hepatic tumor ablation," *Biomedical Engineering, IEEE Transactions on*, vol. 49, no. 1, pp. 3–9, 2002.
- [35] B.-M. Kim, S. L. Jacques, S. Rastegar, S. Thomsen, and M. Motamed, "Nonlinear finite-element analysis of the role of dynamic changes in blood perfusion and optical properties in laser coagulation of tissue," *Selected Topics in Quantum Electronics, IEEE Journal of*, vol. 2, no. 4, pp. 922–933, 1996.
- [36] P. Dorato, V. Cerone, and C. Abdallah, *Linear-quadratic control: an introduction*. Simon & Schuster, 1994.
- [37] J. Nocedal and S. Wright, *Numerical optimization*. Springer Science & Business Media, 2006.